JACS
JOURNAL OF THE AMERICAN CHEMICAL SOCIETY
Article
pubs.acs.org/JACS

Guest-Induced Two-Way Structural Transformation in a Layered Metal–Organic Framework Thin Film

Tomoyuki Haraguchi,[†] Kazuya Otsubo,[*,†] Osami Sakata,[‡] Akihiko Fujiwara,[§] and Hiroshi Kitagawa[*,†,∥,⊥]

[†]Division of Chemistry, Graduate School of Science, Kyoto University, Kitashirakawa-Oiwakecho, Sakyo-ku, Kyoto 606-8502, Japan
[‡]Synchrotron X-ray Station at SPring-8, National Institute for Materials Science (NIMS), 1-1-1 Kouto, Sayo-cho, Sayo-gun, Hyogo 679-5148, Japan
[§]School of Science and Technology, Kwansei Gakuin University, 2-1 Gakuen, Sanda, Hyogo 669-1337, Japan
[∥]Institute for Integrated Cell-Material Sciences (iCeMS), Kyoto University, Yoshida, Sakyo-ku, Kyoto 606-8501, Japan
[⊥]INAMORI Frontier Research Center, Kyushu University, 744 Motooka, Nishi-ku, Fukuoka 819-3095, Japan

Supporting Information

ABSTRACT: Fabrication of thin films made of metal–organic frameworks (MOFs) has been intensively pursued for practical applications that use the structural response of MOFs. However, to date, only physisorption-induced structural response has been studied in these films. Chemisorption can be expected to provide a remarkable structural response because of the formation of bonds between guest molecules and reactive metal sites in host MOFs. Here, we report that chemisorption-induced two-way structural transformation in a nanometer-sized MOF thin film. We prepared a two-dimensional layered-type MOF $Fe[Pt(CN)_4]$ thin film using a step-by-step approach. Although the as-synthesized film showed poor crystallinity, the dehydrated form of this thin film had a highly oriented crystalline nature (**Film-D**) as confirmed by synchrotron X-ray diffraction (XRD). Surprisingly, under water and pyridine vapors, **Film-D** showed chemisorption-induced dynamic structural transformations to $Fe(L)_2[Pt(CN)_4]$ thin films [L = H_2O (**Film-H**), pyridine (**Film-P**)], where water and pyridine coordinated to the open Fe^{2+} site. Dynamic structural transformations were also confirmed by in situ XRD, sorption measurement, and infrared reflection absorption spectroscopy. This is the first report of chemisorption-induced dynamic structural response in a MOF thin film, and it provides useful insights, which would lead to future practical applications of MOFs utilizing chemisorption-induced structural responses.

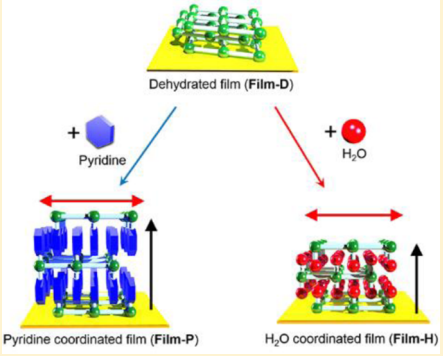

INTRODUCTION

Recent research in metal–organic frameworks (MOFs)[1] has focused on a broad variety of properties such as gas sorption,[2] sensing,[3] catalysis,[4] conductivity,[5] and electrical properties.[6] In contrast to rigid porous inorganic materials such as porous carbon, zeolites, and aluminophosphates,[7] MOFs possess structural flexibility because of the coordination bonds between metal ions and organic ligands that are weaker than covalent bonds; this is the key to a unique structural response upon guest adsorption and an efficient recognition of guest molecules.[8] In addition, such structural flexibility often provides remarkable structural transformations induced by guest adsorption.[9] In recent years, MOF thin films have been intensively explored for practical applications that use the structural response of MOFs, such as high-performance membrane, switching devices, and chemical sensors.[10] To date, various kinds of MOF thin films have been fabricated, and their structural response has been investigated, where in some cases a structural transformation is triggered by guest adsorption on the surface of host frameworks.[11] One example of such a large structural response is the gate-opening phenomenon, in which the sorption profile shows an abrupt increase in adsorption with the rearrangement of the crystal structure from a specific vapor pressure (the gate-opening pressure).[11g,12] However, for MOF thin films, only physisorption-induced structural response has been studied to date; the other type of sorption phenomenon, i.e., chemisorption, has not yet been used in a MOF thin film.[11] In the chemisorption process, a remarkable structural transformation can be expected because of the bond formation between guest molecules and reactive metal sites in host MOFs.[13] In addition, high guest selectivity can also be expected for the chemisorption process because some guest molecules would interact with reactive sites and others would not. For example, a flexible MOF, $Cu_2(OH)(C_8H_3O_7S)(H_2O)\cdot 2H_2O$, is known to show high selectivity toward nitric oxide through a coordination-driven gating mechanism.[13c] We have focused on Hofmann-type MOFs, $Fe(L)_2[Pt(CN)_4]$ (L = ligands), as a candidate for thin-film fabrication; here, ligands coordinate the Fe^{2+} metal sites of

Received: October 18, 2016
Published: December 12, 2016

DOI: 10.1021/jacs.6b10913
J. Am. Chem. Soc. 2016, 138, 16787–16793

cyanide-bridged two-dimensional (2D) layers $Fe[Pt(CN)_4]$ (Figure 1a).[14] This means that a MOF thin film fabricated by layering the cyanide-bridged 2D sheets, $Fe[Pt(CN)_4]$, would be expected to have reactive Fe^{2+} sites. To our knowledge, although ligand coordinated Hofmann-type MOFs are well-known,[14] the ligand coordination process has not yet been observed in a Hofmann-type MOF.

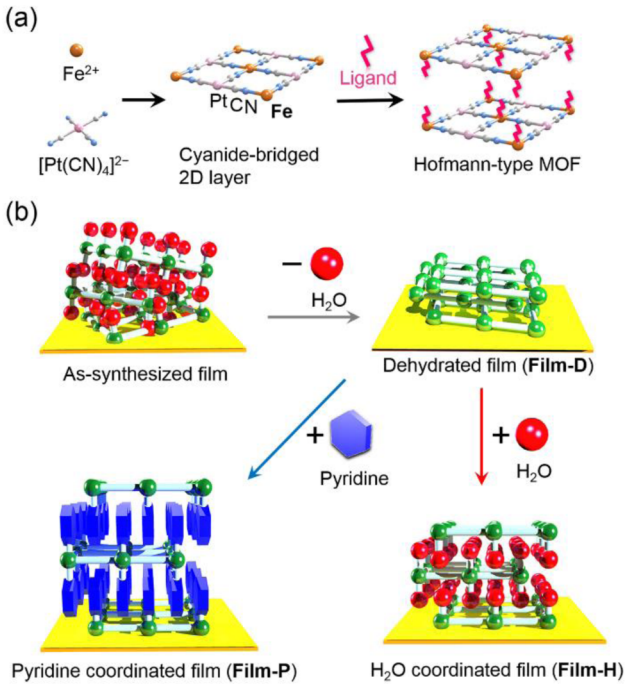

Figure 1. Schematic representations of (a) formation of cyanide-bridged 2D layer and Hofmann-type MOF and (b) two-way structural transformation of a $Fe[Pt(CN)_4]$ thin film (**Film-D**) induced by coordination of water and pyridine molecules.

Here, we report on chemisorption-induced dynamic structural transformations in a nanometer-size MOF thin film. Using a step-by-step approach, we constructed a 2D-layered MOF thin film, $Fe[Pt(CN)_4]$. Although the as-synthesized film showed poor crystallinity, simple dehydration of this film provided a highly oriented crystalline $Fe[Pt(CN)_4]$ thin film (**Film-D**). The sorption isotherms of **Film-D** showed abrupt uptakes upon water and pyridine vapor adsorption. A synchrotron X-ray diffraction (XRD) study revealed not only the highly oriented crystalline nature but also the dynamic structural transformation. **Film-D** transformed to the H_2O coordinated form (**Film-H**) and pyridine coordinated form (**Film-P**) induced by coordination of water and pyridine molecules to the open Fe^{2+} sites (Figure 1b). This is the first report of a chemisorption-induced dynamic structural response in a MOF thin film.

EXPERIMENTAL SECTION

Materials. 4-Mercaptopyridine, $Fe(BF_4)_2{\cdot}6H_2O$, $K_2[Pt(CN)_4]{\cdot}H_2O$, $[(C_4H_9)_4N]ClO_4$, ethanol, acetone, and diethyl ether were purchased from Sigma-Aldrich Chemical Corp., Tokyo Kasei Kogyo Corp. Ltd., or Kishida Chemical Corp. Ltd. These materials were used without any further purification. The substrate (Au/Cr/Si) was purchased from Nilaco Corp., which was prepared by evaporating 5 nm of Cr followed by 100 nm of Au onto a Si wafer. The substrate was used after washing with pure ethanol and H_2-annealing treatment. The starting material, $[(C_4H_9)_4N]_2[Pt(CN)_4]$, was prepared according to the previous report[11c] through the equimolar cation-exchange reaction of $K_2[Pt(CN)_4]$ and $[(C_4H_9)_4N]ClO_4$ in ethanol for 1 week and was purified by the recrystallization from acetone and diethyl ether.

Preparation of Thin Films. The Au/Cr/Si substrate (15 × 15 × 0.5 mm^3) was immersed in an ethanol solution of 4-mercaptopyridine (1 mM) overnight, and then, the substrate was functionalized with a self-assembled monolayer. Next, the substrate was washed with pure ethanol and dried under a N_2 gas stream. The substrate was then immersed alternately in ethanol solutions of $Fe(BF_4)_2{\cdot}6H_2O$ (5 mM) and $[(C_4H_9)_4N]_2Pt(CN)_4$ (5 mM) for 5 min at −60 °C, for 30 steps. Finally, the substrate was washed with pure ethanol and dried under a N_2 gas stream.

Synthesis of Bulk $Fe[Pt(CN)_4]$. Bulk $Fe[Pt(CN)_4]$ was synthesized by mixing ethanol solutions of $Fe(BF_4)_2{\cdot}6H_2O$ (319 mg, 10 mM) and $[(C_4H_9)_4N]_2[Pt(CN)_4]$ (135 mg, 10 mM). The synthesized white powder was washed with ethanol and collected by centrifuging. Anal. (%) Calcd for $Fe[Pt(CN)_4]{\cdot}4H_2O{\cdot}0.3C_2H_5OH$: C, 12.53; H, 2.24; N, 12.71. Found: C, 12.42; H, 2.01; N, 12.57.

Characterization of Thin Films. The formation of the thin films was confirmed by infrared (IR) reflection absorption spectra (IRRAS). The sorption properties of the dehydrated film (**Film-D**) were investigated by quartz crystal microbalance (QCM) measurements with a BELQCM system (MicrotracBEL). Before the measurements, the QCM sensors were activated at 80 °C for 1 day under a He gas stream inside the QCM chamber. Atomic force microscopy (AFM) images of **Film-D**, **Film-H**, and **Film-P** were obtained in the tapping mode with a NanoScope IIIa system (Veeco Instrument Inc.).

Synchrotron XRD Measurements and in Situ Synchrotron XRD Measurements of Thin Films. Synchrotron XRD measurements were carried out on the BL13XU beamline of SPring-8 (Hyogo, Japan) using a multiaxis diffractometer (Kohzu−Seiki TDT-17) with a scintillation detector for different scattering geometries: the vertical direction (out-of-plane, θ–2θ mode) and the horizontal direction (in-plane, θ fixed 2θ mode) relative to the substrate. The incident X-ray was monochromatized to 8 keV (λ = 1.550 Å, room temperature (rt)). He gas was supplied during the measurements. Out-of-plane XRD measurements were performed in a typical θ–2θ scattering geometry. In grazing-incidence XRD (GIXRD, in-plane mode), a strong scattered intensity could be observed when the X-ray incident angle (α) to the sample was below a critical angle. Thus, the GIXRD measurement at the 100 peak position was performed before the in-plane XRD measurement, and the diffraction patterns were collected at α = 0.2°. A Soller slit (Huber 3030-I, 0.4°) was placed between the sample substrate and the scintillation detector to reduce scatter background from the diffraction. XRD pattern fittings were performed using the Topas program.[15] Simulated XRD patterns were obtained with the Mercury software suite.[16] For in situ XRD measurements of the thin films, the vapor pressure was controlled by using a BEL-Flow system (MicrotracBEL).

RESULTS AND DISCUSSION

Thin Film Preparation and Characterization. The thin films were prepared using a step-by-step approach. First, the Au/Cr/Si substrate was immersed in an ethanol solution of 4-mercaptopyridine (1 mM) overnight, and then the substrate was functionalized with a self-assembled monolayer. The substrates were then washed with pure ethanol and dried under a nitrogen gas stream. The substrates were then alternately immersed in ethanol solutions of $Fe(BF_4)_2{\cdot}6H_2O$ and $[(C_4H_9)_4N]_2Pt(CN)_4$ at −60 °C, for a total of 30 steps. Finally, the substrates were washed with pure ethanol and dried under a nitrogen gas stream. To confirm thin-film growth, IRRAS measurements were carried out at rt. Thin-film growth was monitored by IRRAS after each fabrication step (Figure 2a,b). The peak intensity of the ν(CN) stretching mode linearly increased with the number of fabrication steps, indicating a successive thin-film growth on the surface of the substrate. Furthermore, as shown in Figure 2c, sharp ν(OH) stretching,

DOI: 10.1021/jacs.6b10913
J. Am. Chem. Soc. 2016, 138, 16787−16793

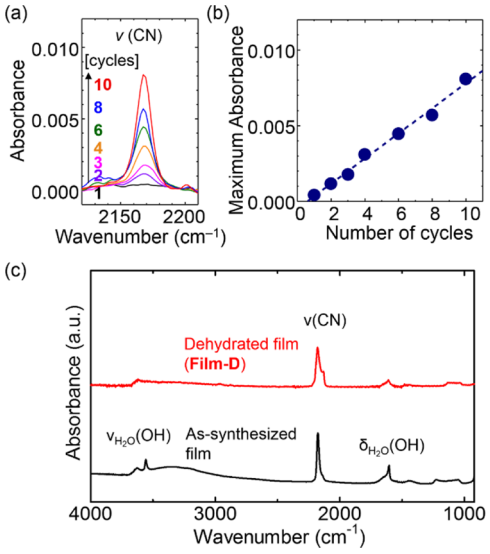

Figure 2. (a) Successive thin-film growth of an as-synthesized film monitored by IRRAS. (b) Dependence of the maximum absorbance of the ν(CN) stretching mode in part a. The blue dotted line is a least-squares fitting. (c) IRRAS of as-synthesized film and dehydrated film (**Film-D**).

δ(OH) bending, and ν(CN) stretching modes were observed on the as-synthesized film, which suggested that this film contained H_2O and the CN group.

In general, low electron density and the thickness of the MOF thin films make it difficult to confirm the structure using conventional XRD. For such cases, synchrotron XRD is a powerful technique because of the high photon flux density. To confirm crystallinity and orientation of the thin films, synchrotron XRD measurements were performed at the BL13XU beamline of SPring-8 (λ = 1.550 Å, rt). Figure 3 shows synchrotron XRD profiles of an as-synthesized film for different scattering geometries: the vertical direction (out-of-plane, θ–2θ mode; Figure 3a) and the horizontal direction (in-plane, 2θ mode; Figure 3b) relative to the substrate. A single peak, which would correspond to the interlayer spacing, was observed for the out-of-plane geometry. On the other hand, several peaks were observed for in-plane geometry, which would correspond to the intralayer ordering. However, the obtained patterns of the as-synthesized film exhibited poor crystallinity, and indexing of the diffraction patterns was unsuccessful. For comparison, a bulk sample was synthesized by simple mixing of the structural components and was characterized by elemental analysis (see the Experimental Section). It should be noted that the patterns of the as-synthesized film were similar to those of the bulk sample (Figure S1). Surprisingly, after a simple dehydration process under evacuation at 80 °C for the as-synthesized film, crystallinity was significantly improved (**Film-D**). In addition, shifts of all diffraction peaks to the higher angle side were observed, which would be due to structural shrinkage induced by water removal. As shown in Figure 1b, the as-synthesized film would be fabricated in a disordered manner, and the layers would be separated by coordinated waters and guest molecules. After water removal by a heating procedure, the separated layers would be stacked via van der Waals interaction between layers. As a result of this process, the improvement of the crystallinity and the orientation in **Film-D** compared with those of the as-synthesized film would occur. The crystal structure of

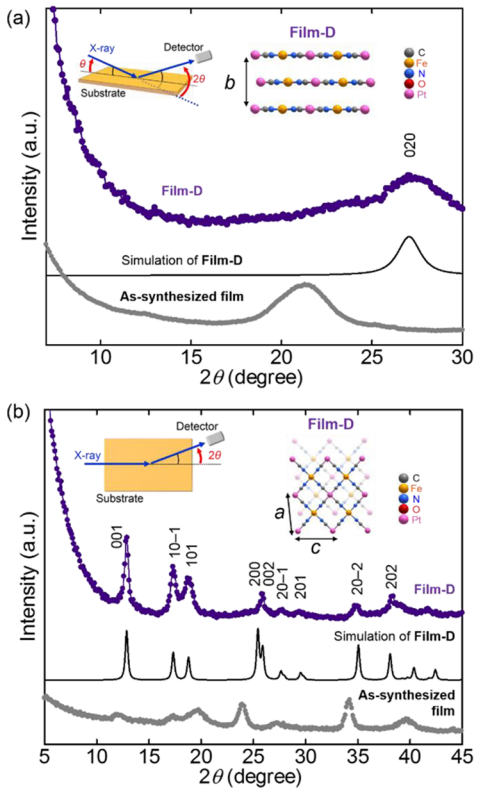

Figure 3. Synchrotron XRD patterns of as-synthesized film and **Film-D** (λ = 1.550 Å, rt). (a) Out-of-plane (θ–2θ mode) XRD patterns. (b) In-plane (θ fixed 2θ mode) XRD patterns. Filled circles and black lines denote experimental data and simulated diffraction patterns, respectively. Inset figures in each panel denote the scattering geometries of the XRD study (left) and the modeled structures (right).

the water coordinated Hofmann-type MOF analogue, Fe$(H_2O)_2[Ni(CN)_4]\cdot 2$(1,4-dioxane) (Figure S2), was reported (monoclinic, $P2/m$).[17] Thus, on the basis of the single-crystal X-ray structure of Fe$(H_2O)_2[Ni(CN)_4]\cdot 2$(1,4-dioxane), we constructed a modeled crystal structure for **Film-D** (insets of Figure 3, a monoclinic unit cell, $P2_1/m$). The diffraction peaks of **Film-D** agreed well with the AB packing simulation patterns of a monoclinic structure ($P2_1/m$, a = 7.050(7) Å, b = 6.59(3) Å, c = 6.946(4) Å, β = 94.59(5)°), whereas the AA packing model showed poor agreement with the diffraction peaks (Figure S3). Removal of water was also confirmed by IRRAS; the ν(OH) stretching and δ(OH) bending modes were not observed after the dehydration process (Figure 2c).

Sorption Properties of Film-D. Next, we investigated sorption isotherms of **Film-D** by QCM measurements (Figure 4). The measurements were performed after dehydration of the as-synthesized film by heating at 80 °C for 1 day under a He gas stream inside the QCM chamber. The pyridine sorption isotherm exhibited an abrupt uptake of ~2 pyridine molecules per one Fe at P/P_0 = ~0.9 with wide hysteresis. In contrast, the water sorption isotherm exhibited a complicated sorption behavior; an abrupt uptake of ~7 water molecules per one Fe was observed at P/P_0 = ~0.6, whereas ~5 water molecules desorbed and ~2 water molecules remained after the adsorption process with wide hysteresis (vide infra). In contrast, no significant uptake was observed for methanol, ethanol, acetonitrile, and benzene, except for small adsorption to the surface and domain boundary in the MOF thin film in the high-pressure region. It should be noted that two molecules

DOI: 10.1021/jacs.6b10913
J. Am. Chem. Soc. 2016, 138, 16787–16793

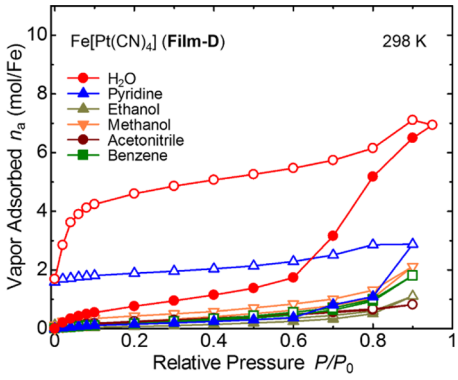

Figure 4. H_2O and pyridine adsorption/desorption isotherms of a dehydrated thin film (**Film-D**) obtained from QCM measurements at rt. Filled symbols and open symbols denote adsorption and desorption, respectively.

remained per one Fe after the desorption process only for water and pyridine vapors. This feature suggested a relatively strong coordination (chemisorption) of the molecules to open Fe^{2+} sites. The highly selective adsorption of water and pyridine is particularly noteworthy in that significant adsorption did not occur for molecules of similar shapes such as methanol and benzene.

Dynamic Structural Transformations of Film-D under Water and Pyridine Vapors. From the sorption measurements, large structural responses were expected for **Film-D** under water and pyridine vapors, and thus, synchrotron XRD measurements were performed. The synchrotron XRD profiles of **Films-D**, **-H**, and **-P** for out-of-plane and in-plane geometries are shown in Figure 5. The XRD patterns of **Film-P** were the same as those of the $Fe(py)_2[Pt(CN)_4]$ thin film (py: pyridine), on which we reported recently,[11g] indicating that **Film-P** has the same crystal structure and oriented nature as the $Fe(py)_2[Pt(CN)_4]$ thin film. As shown in Figure 5, we constructed a model structure for **Film-H** based on the single-crystal X-ray structure of $Fe(py)_2[Pt(CN)_4]$ (orthorhombic, *Cmmm*).[11g] Both diffraction peaks of **Film-H** and **Film-P** agreed well with AB packing simulation patterns of orthorhombic symmetries (*Pmmm*, a = 7.319(6) Å, b = 7.44(3) Å, c = 7.375(6) Å for **Film-H**; *Cmmm*, a = 7.43(3) Å, b = 15.306(3) Å, c = 7.37(3) Å for **Film-P**), whereas the AA packing model showed poor agreement with the diffraction peaks (Figures S4 and S5). The synchrotron X-ray study clearly demonstrated that **Film-D** showed a chemisorption-induced structural transformation to two-molecule coordinated structures, **Film-H** and **Film-P**, which had high crystallinity and well-controlled orientations of the crystal growth in both out-of-plane and in-plane directions. This is consistent with the results of sorption measurements where two molecules per one Fe remained after the desorption process. Two peaks assignable to the 111 and 311 diffraction peaks were observed in **Film-P** because of its canted nature, which were also observed in an $Fe(py)_2[Pt(CN)_4]$ thin film in our previous work.[11g] The absence of azimuthal angle dependence within the surface plane (Figures S7–9) implies that films are formed uniformly without any preferential direction on the substrates. The crystalline domain sizes (D) were estimated using the Scherrer equation from 001 or 100 (in-plane, D_{in}) and 020 (out-of-plane, D_{out}) peaks (D_{in} = 21 nm, D_{out} = 3 nm for **Film-D**; D_{in} = 17 nm, D_{out} = 3 nm for **Film-H**; D_{in} = 14 nm, D_{out} = 7 nm for **Film-P**). In contrast, AFM images of **Film-D**, **Film-H**, and **Film-P** revealed

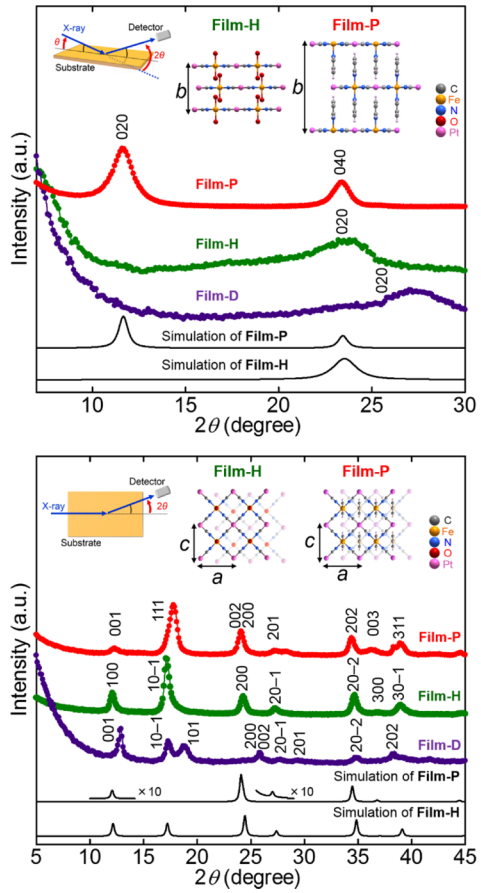

Figure 5. Synchrotron XRD patterns of **Film-D**, **Film-H**, and **Film-P** (λ = 1.550 Å, rt). (a) Out-of-plane (θ–2θ mode) XRD patterns. (b) In-plane (θ fixed 2θ mode) XRD patterns. Filled circles and black lines denote experimental data and simulated diffraction patterns, respectively. Inset figures in each panel denote the scattering geometries of the XRD study (left) and the modeled structures (right).

several domains (Figures S10–12); both large (~300 nm) and small (<50 nm) domains existed for the three films, and no significant morphology change was observed after the hydration and pyridine adsorption processes for **Film-D**. Thus, because of the large domain size dispersion, the crystalline domain sizes calculated by XRD would be smaller than those determined from AFM observation. It should be noted that the structural response was observed not only in the out-of-plane direction but also in the in-plane direction. To our knowledge, only anisotropic changes in the out-of-plane direction have been observed for physisorption-induced structural response in highly oriented crystalline MOF thin films,[11] which may be due to the strong stacking interaction among layers in the frameworks. Moreover, the large structural transformation from **Film-D** to **Film-P** (132% increase of lattice b) on the surface is also a remarkable result. To our knowledge, only several percent of structural changes have been reported for highly oriented crystalline MOF thin films at most.[11] Structural transformations from **Film-D** to **Film-H** and **Film-P** were also confirmed by IRRAS. As shown in Figure 6, the ν(OH) stretching and δ(OH) bending modes were observed after hydration, and ν(ring) stretching and δ(CH) bending modes were observed after the pyridine adsorption process. These observed sharp vibrational modes indicated water and pyridine coordination to open Fe^{2+} sites.

DOI: 10.1021/jacs.6b10913
J. Am. Chem. Soc. 2016, 138, 16787–16793

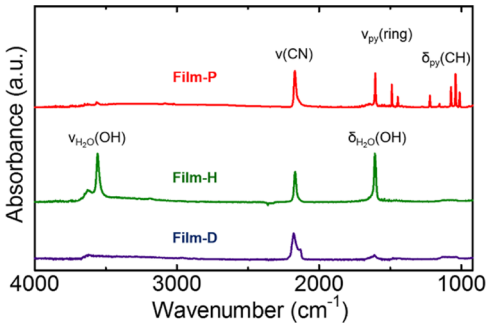

Figure 6. IRRAS of **Film-D**, **Film-H**, and **Film-P**.

Relationship between Water Sorption Behavior and Structural Transformation from Film-D to Film-H. As described above, the complicated sorption behavior of **Film-D** followed by structural transformation to **Film-H** was observed under water vapor. Thus, the structural transformation process upon water adsorption was investigated in detail using in situ XRD measurements (Figure 7). During water adsorption, the

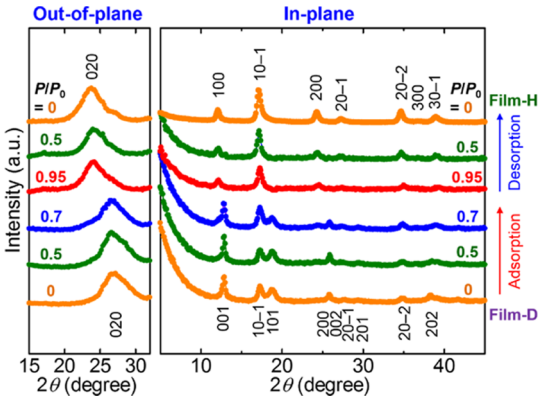

Figure 7. In situ synchrotron XRD patterns of the dehydrated thin film (**Film-D**) under water vapor at 298 K.

diffraction peaks from **Film-H** began to appear at P/P_0 = 0.7 in addition to the diffraction pattern from **Film-D**. The diffraction peaks completely changed at P/P_0 = 0.95, and the diffraction peaks of **Film-H** were maintained even after the desorption process, indicating that the structural transformation was irreversible because of the formation of a coordination bond between water molecules and Fe^{2+}. The dependence of the lattice constants on water vapor pressure was determined by Le Bail fitting of the diffraction patterns (Figure 8). The lattice parameter b corresponding to the interlayer spacing was determined using in situ out-of-plane synchrotron X-ray measurements. Other parameters a, c, and β, which correspond to the intralayer structure, were determined from in situ in-plane synchrotron X-ray measurements. All lattice parameters were determined considering the monoclinic and the orthorhombic structure models described above upon adsorption/desorption processes. The water sorption isotherms of the first and second cycle are also shown for comparison. As is clearly seen, abrupt lattice changes were observed at P/P_0 = 0.9 with large hysteresis. In contrast, almost no lattice change was observed under the desorption process. This indicates that desorption of ∼5 water molecules (observed from QCM measurement of the first cycle under the desorption process) could be assigned to the removal of crystal water and of water

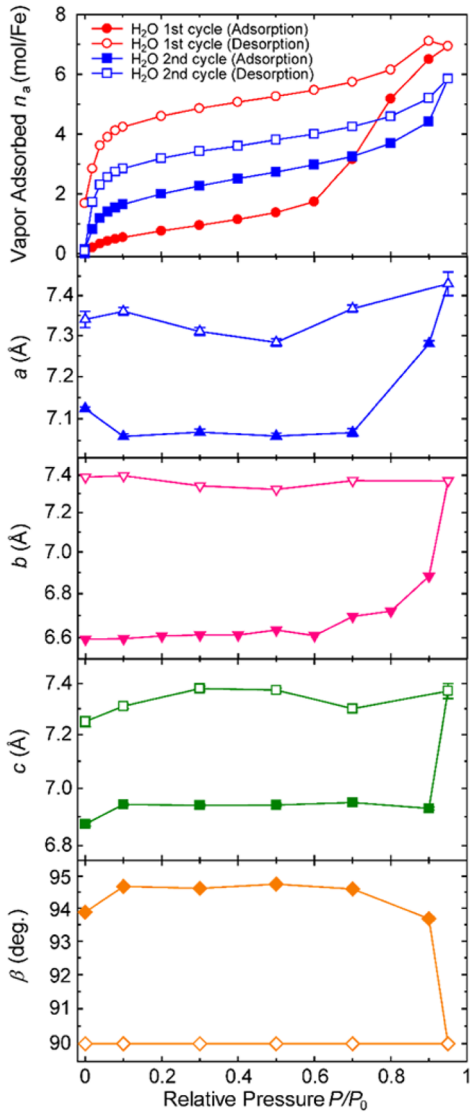

Figure 8. Sorption isotherm of H_2O and changes in lattice constants obtained from in situ synchrotron XRD of the dehydrated thin film (**Film-D**) at 298 K. Filled and open symbols denote the adsorption and desorption processes, respectively. All cell parameters were determined considering the monoclinic and orthorhombic structure models under the adsorption and desorption processes, respectively.

adsorbed on the surface and domain boundary, which did not contribute to the structural changes of **Film-H**. This assignment is also supported by the results of the water sorption isotherm of the second cycle (Figure 8); the isotherm exhibited type I sorption profiles typical for microporous materials in the IUPAC classification[13a,b] with uptake of ∼5 water molecules (assignable to ∼2 crystal waters in the low-pressure region and ∼3 waters adsorbed on the surface and domain boundary).

CONCLUSION

In conclusion, we have demonstrated that chemisorption induced a two-way structural transformation in a nanometer-sized MOF thin film. Synchrotron XRD revealed a dynamic structural transformation from **Film-D** to water and pyridine coordinated films. The sorption isotherms of **Film-D** showed abrupt uptakes upon water and pyridine vapor adsorption. This is the first report of a chemisorption-induced dynamic

DOI: 10.1021/jacs.6b10913
J. Am. Chem. Soc. 2016, 138, 16787−16793

structural response in a MOF thin film. These results could provide useful insights, which would lead to future practical applications of MOFs utilizing chemisorption-induced structural responses.

■ ASSOCIATED CONTENT

Supporting Information

The Supporting Information is available free of charge on the ACS Publications website at DOI: 10.1021/jacs.6b10913.

Details of experimental procedures, additional XRD data, Raman spectra, and AFM images (PDF)

■ AUTHOR INFORMATION

Corresponding Authors

*kazuya@kuchem.kyoto-u.ac.jp

*kitagawa@kuchem.kyoto-u.ac.jp

ORCID

Hiroshi Kitagawa: 0000-0001-6955-3015

Notes

The authors declare no competing financial interest.

■ ACKNOWLEDGMENTS

This work was supported by Core Research for Evolutional Science and Technology (CREST) and ACCEL from the Japan Science and Technology Agency (JST), Grants-in-Aid for Scientific Research (A) (Grant Nos. 20350030 and 23245012), Grant-in-Aid for Young Scientists (B) (Grant No. 25810039), and Grants-in-Aid for JSPS Fellows (25-1768) from the Japan Society for the Promotion of Science (JSPS). Synchrotron XRD measurements were supported by the Japan Synchrotron Radiation Research Institute (JASRI) (Proposal Nos. 2014A1419, 2014B1443, 2015A1489, 2015B1537, 2016A1421).

■ REFERENCES

(1) (a) Furukawa, H.; Cordova, K. E.; O'Keeffe, M.; Yaghi, O. M. *Science* **2013**, *341*, 1230444-1−1230444-12. (b) Kitagawa, S.; Kitaura, R.; Noro, S. *Angew. Chem., Int. Ed.* **2004**, *43*, 2334−2375. (c) Yaghi, O. M.; O'Keeffe, M.; Ockwig, N. W.; Chae, H. K.; Eddaoudi, M.; Kim, J. *Nature* **2003**, *423*, 705−714. (d) Férey, G. *Chem. Soc. Rev.* **2008**, *37*, 191−214. (e) James, S. L. *Chem. Soc. Rev.* **2003**, *32*, 276−288. (f) Shimizu, G. K. H.; Vaidhyanathan, R.; Taylor, J. M. *Chem. Soc. Rev.* **2009**, *38*, 1430−1449. (g) Cohen, S. M. *Chem. Rev.* **2012**, *112*, 970−1000.

(2) (a) Chae, H. K.; Siberio-Perez, D. Y.; Kim, J.; Go, Y.; Eddaoudi, M.; Matzger, A. J.; O'Keeffe, M.; Yaghi, O. M. *Nature* **2004**, *427*, 523−527. (b) Li, J. R.; Kuppler, R. J.; Zhou, H.-C. *Chem. Soc. Rev.* **2009**, *38*, 1477−1504. (c) Li, J.-R.; Sculley, J.; Zhou, H.-C. *Chem. Rev.* **2012**, *112*, 869−932.

(3) (a) Lee, J.; Farha, O. K.; Roberts, J.; Scheidt, K. A.; Nguyen, S. T.; Hupp, J. T. *Chem. Soc. Rev.* **2009**, *38*, 1450−1459. (b) Yoon, M.; Srirambalaji, R.; Kim, K. *Chem. Rev.* **2012**, *112*, 1196−1231.

(4) Kreno, L. E.; Leong, K.; Farha, O. K.; Allendorf, M.; Van Duyne, R. P.; Hupp, J. T. *Chem. Rev.* **2012**, *112*, 1105−1125.

(5) (a) Otsubo, K.; Kobayashi, A.; Kitagawa, H.; Hedo, M.; Uwatoko, Y.; Sagayama, H.; Wakabayashi, Y.; Sawa, H. *J. Am. Chem. Soc.* **2006**, *128*, 8140−8141. (b) Sadakiyo, M.; Ōkawa, H.; Shigematsu, A.; Ohba, M.; Yamada, T.; Kitagawa, H. *J. Am. Chem. Soc.* **2012**, *134*, 5472−5475.

(6) (a) Kurmoo, M. *Chem. Soc. Rev.* **2009**, *38*, 1353−1379. (b) Ōkawa, H.; Shigematsu, A.; Sadakiyo, M.; Miyagawa, T.; Yoneda, K.; Ohba, M.; Kitagawa, H. *J. Am. Chem. Soc.* **2009**, *131*, 13516−13522. (c) Otsubo, K.; Wakabayashi, Y.; Ohara, J.; Yamamoto, S.; Matsuzaki, H.; Okamoto, H.; Nitta, K.; Uruga, T.; Kitagawa, H. *Nat. Mater.* **2011**, *10*, 291−295. (d) Otsubo, K.; Kobayashi, A.; Sugimoto, K.; Fujiwara, A.; Kitagawa, H. *Inorg. Chem.* **2014**, *53*, 1229−1240. (e) Otsubo, K.; Kitagawa, H. *CrystEngComm* **2014**, *16*, 6277−6286. (f) Otake, K.; Otsubo, K.; Sugimoto, K.; Fujiwara, A.; Kitagawa, H. *Angew. Chem., Int. Ed.* **2016**, *55*, 6448−6451. (g) Otake, K.; Otsubo, K.; Sugimoto, K.; Fujiwara, A.; Kitagawa, H. *Inorg. Chem.* **2016**, *55*, 2620−2626.

(7) (a) Davis, M. E. *Nature* **2002**, *417*, 813−821. (b) Pastore, H. O.; Coluccia, S.; Marchese, L. *Annu. Rev. Mater. Res.* **2005**, *35*, 351−395.

(8) Horike, S.; Shimomura, S.; Kitagawa, S. *Nat. Chem.* **2009**, *1*, 695−704. (b) Fletcher, A. J.; Thomas, K. M.; Rosseinsky, M. J. *J. Solid State Chem.* **2005**, *178*, 2491−2510. (c) Uemura, K.; Matsuda, R.; Kitagawa, S. *J. Solid State Chem.* **2005**, *178*, 2420−2429.

(9) (a) Krause, S.; Bon, V.; Senkovska, I.; Stoeck, U.; Wallacher, D.; Többens, D. M.; Zander, S.; Pillai, R. S.; Maurin, G.; Coudert, F.-X.; Kaskel, S. *Nature* **2016**, *532*, 348−352. (b) Llewellyn, P. L.; Bourrelly, S.; Serre, C.; Filinchuk, Y.; Férey, G. *Angew. Chem., Int. Ed.* **2006**, *45*, 7751−7754.

(10) (a) Zacher, D.; Schmid, R.; Wöll, C.; Fischer, R. A. *Angew. Chem., Int. Ed.* **2011**, *50*, 176−199. (b) Shekhah, O.; Liu, J.; Fischer, R. A.; Wöll, C. *Chem. Soc. Rev.* **2011**, *40*, 1081−1106. (c) Bétard, A.; Fischer, R. A. *Chem. Rev.* **2012**, *112*, 1055−1083. (d) Zhuang, J.-L.; Terfort, A.; Wöll, C. *Coord. Chem. Rev.* **2016**, *307*, 391−424.

(11) (a) Scherb, C.; Schödel, A.; Bein, T. *Angew. Chem., Int. Ed.* **2008**, *47*, 5777−5779. (b) Scherb, C.; Koehn, R.; Bein, T. *J. Mater. Chem.* **2010**, *20*, 3046−3051. (c) Otsubo, K.; Haraguchi, T.; Sakata, O.; Fujiwara, A.; Kitagawa, H. *J. Am. Chem. Soc.* **2012**, *134*, 9605−9608. (d) Otsubo, K.; Kitagawa, H. *APL Mater.* **2014**, *2*, 124105-1−124105-11. (e) Haraguchi, T.; Otsubo, K.; Sakata, O.; Fujiwara, A.; Kitagawa, H. *Inorg. Chem.* **2015**, *54*, 11593−11595. (f) Haraguchi, T.; Otsubo, K.; Sakata, O.; Kawaguchi, S.; Fujiwara, A.; Kitagawa, H. *Chem. Commun.* **2016**, *52*, 6017−6020. (g) Sakaida, S.; Otsubo, K.; Sakata, O.; Song, C.; Fujiwara, A.; Takata, M.; Kitagawa, H. *Nat. Chem.* **2016**, *8*, 377−383.

(12) (a) Serre, C.; Millange, F.; Thouvenot, C.; Noguès, M.; Marsolier, G.; Louër, D.; Férey, G. *J. Am. Chem. Soc.* **2002**, *124*, 13519−13526. (b) Kitaura, R.; Seki, K.; Akiyama, G.; Kitagawa, S. *Angew. Chem., Int. Ed.* **2003**, *42*, 428−431. (c) Matsuda, R.; Kitaura, R.; Kitagawa, S.; Kubota, Y.; Kobayashi, T. C.; Horike, S.; Takata, M. *J. Am. Chem. Soc.* **2004**, *126*, 14063−14070. (d) Chen, B.; Liang, C.; Yang, J.; Contreras, D. S.; Clancy, Y. L.; Lobkovsky, E. B.; Yaghi, O. M.; Dai, S. *Angew. Chem., Int. Ed.* **2006**, *45*, 1390−1393.

(13) (a) Sing, K. S. W.; Everett, D. H.; Haul, R. A. W.; Moscou, L.; Pierotti, R. A.; Rouquerol, J.; Siemieniewska, T. *Pure Appl. Chem.* **1985**, *57*, 603−619. (b) Gregg, S. J.; Sing, K. S. W. *Adsorption, Surface Area and Porosity*; Academic Press: London, 1982; Chapter 3.5, p 172. (c) Xiao, B.; Byrne, P. J.; Wheatley, P. S.; Wragg, D. S.; Zhao, X.; Fletcher, A. J.; Thomas, K. M.; Peters, L.; Evans, J. S. O.; Warren, J. E.; Zhou, W.; Morris, R. E. *Nat. Chem.* **2009**, *1*, 289−294. (d) Cussen, E. J.; Claridge, J. B.; Rosseinsky, M. J.; Kepert, C. J. *J. Am. Chem. Soc.* **2002**, *124*, 9574−9581. (e) Bhattacharya, B.; Halder, A.; Maity, D. K.; Ghoshal, D. *CrystEngComm* **2016**, *18*, 4074−4083.

(14) (a) Niel, V.; Martínez-Agudo, J. M.; Muñoz, M. C.; Gaspar, A. B.; Real, J. A. *Inorg. Chem.* **2001**, *40*, 3838−3839. (b) Culp, J. T.; Smith, M. R.; Bittner, E.; Bockrath, B. *J. Am. Chem. Soc.* **2008**, *130*, 12427−12434. (c) Ohba, M.; Yoneda, K.; Agustí, G.; Muñoz, M. C.; Gaspar, A. B.; Real, J. A.; Yamasaki, M.; Ando, H.; Nakao, Y.; Sakaki, S.; Kitagawa, S. *Angew. Chem., Int. Ed.* **2009**, *48*, 4767−4771. (d) Southon, P. D.; Liu, L.; Fellows, E. A.; Price, D. J.; Halder, G. J.; Chapman, K. W.; Moubaraki, B.; Murray, K. S.; Letard, J. F.; Kepert, C. J. *J. Am. Chem. Soc.* **2009**, *131*, 10998−11009. (e) Ohtani, R.; Arai, M.; Ohba, H.; Hori, A.; Takata, M.; Kitagawa, S.; Ohba, M. *Eur. J. Inorg. Chem.* **2013**, *2013*, 738−744. (f) Peng, H.; Tricard, S.; Félix, G.; Molnár, G.; Nicolazzi, W.; Salmon, L.; Bousseksou, A. *Angew. Chem., Int. Ed.* **2014**, *53*, 10894−10898.

(15) Bruker AXS. *TOPAS V3: General Profile and Structure Analysis Software for Powder Diffraction Data*; Bruker AXS: Karlsruhe, Germany, 2005.

(16) Macrae, C. F.; Edgington, P. R.; McCabe, P.; Pidcock, E.; Shields, G. P.; Taylor, R.; Towler, M.; van de Streek, J. *J. Appl. Crystallogr.* **2006**, *39*, 453−457.
(17) Kitazawa, T.; Fukunaga, M.; Takahashi, M.; Takeda, M. *Mol. Cryst. Liq. Cryst. Sci. Technol., Sect. A* **1994**, *244*, 331−336.

DOI: 10.1021/jacs.6b10913
J. Am. Chem. Soc. 2016, 138, 16787−16793